Available online at www.sciencedirect.com

ScienceDirect

IFAC Papers Online CONFERENCE PAPER ARCHIVE

IFAC PapersOnLine 53-2 (2020) 10141–10147

Robust Markovian Impedance Control applied to a Modular Knee-Exoskeleton ⋆

Felix M. Escalante *,** **Juan C. Pérez-Ibarra** *,**
Jonathan C. Jaimes ** **Adriano A. G. Siqueira** **
Marco H. Terra *

* *Department of Electrical Engineering, University of São Paulo at São Carlos, Brazil. (e-mail: maurinho707@usp.br, jcperezibarra@sc.usp.br, terra@sc.usp.br)*

** *Department of Mechanical Engineering, University of São Paulo at São Carlos, Brazil. (e-mail: jonathancj@usp.br, siqueira@sc.usp.br)*

Abstract: Lower limb exoskeletons have improved mobility and safety during gait rehabilitation. Joint actuators can be programmed to produce sufficient joint torque to promote human movement. However, the mechanical impedance of the human joints changes constantly to maintain a stable interaction with the environment during walking. These continuous changes introduce nonlinearities and uncertainties that alter abruptly the dynamics of the human-robot interaction, which can destabilize the control system. In this paper, an impedance control approach under explicit Markovian torque control architecture is developed, considering the variable human impedance parameters as parametric uncertainties. As the time-varying human dynamics during walking depends on the quasi-cyclic gait phase transitions, we defined five Markovian operation modes to describe the human-robot interaction during walking. Additionally, impedance parameters of the human knee joint were estimated using an ensemble-based method. Experimental results of the proposed control scheme on a knee-exoskeleton driven by a series elastic actuator show that our proposal guarantees stability and high performance despite the stochastic uncertain human impedance behavior throughout the gait cycle.

Keywords: Markovian control, Robust control, Impedance control, Human-robot interaction.

1. INTRODUCTION

Human safety is one key challenge when addressing Human-Robot Interaction (HRI) due to the severe implications of human and robot sharing the same work-space, leading even to physical damage (Lasota et al., 2017). In robotic rehabilitation, for example, human and robotic devices constantly exchange energy. From the point of view of the hardware, the use of Series Elastic actuators (SEA) has enhanced the compliance of the robotic devices (Calanca et al., 2016). Those devices normally are driven by impedance controllers that guarantee harmonious interaction (Hogan, 1985; Anam and Al-Jumaily, 2012; Yu et al., 2015). However, due to variability and uncertainty of the human dynamics, stable and secure interaction is not guaranteed. From a control system point-of-view, combined human-robot dynamics constitutes a closed-loop feedback system, where excessive energy exchange may cause degradation of the performance or even instability.

Adaptive Impedance Control (AIC) is an increasingly used solution for the SEA's control problem. Some literature approaches to address this issue consider parameter variation of the human dynamics within its control schematic (Calanca and Fiorini, 2017), and other methods propose to study robot's parameter estimation (Li et al., 2017). In the former, human dynamics have been represented by approximate mass-only models (Kong et al., 2009), or second-order models (with stiffness, damping, and inertia) (Oh and Kong, 2016). Other approaches propose the use of disturbance observers to attenuate non-modeled dynamics effects (Paine et al., 2015), and to improve the transmission of desired impedance (Mehling et al., 2015). However, abrupt changes of the human dynamics during gait can compromise the controller performance. Hence, a better representation of the human dynamics is desirable.

As part of our on-going efforts in the design of robotic devices for assistance and rehabilitation, we developed an impedance-controlled knee orthosis based on a Series Elastic Actuator (dos Santos et al., 2017; dos Santos and Siqueira, 2019). Impedance control of SEAs requires an explicit internal force/torque control loop (Calanca et al., 2016). Previously, we demonstrate that there exists a direct dependence of the performance of these impedance and torque controllers on the variations of the human dynamics (Jutinico et al., 2017), and that a fixed-gain control strategy will suffer degradation of its performance when those variations are not taken into account (Pérez-Ibarra et al., 2017). In this study, we aim to enhance the performance of both impedance and torque controllers

⋆ This work is supported by Pro-Rectory of Research of University of São Paulo, Coordination for the Improvement of Higher Education Personnel (CAPES) - Finance Code 001, Colciencias (Colombia), National Council for Scientific and Technological Development (CNPq), and São Paulo Research Foundation (FAPESP).

10.1016/j.ifacol.2020.12.2740

during walking by considering the abrupt changes in the human dynamics among the different gait phases.

Using a Robust Markovian Linear Regulator approach (Cerri and Terra, 2017), we address the non-linearities and uncertainties proper of the HRI problem from a stochastic point of view. We consider a time-varying dynamics model dependent on quasi-cyclic gait phase transitions during walking. We adapt the methodology proposed in Lee and Hogan (2015) to estimate the human impedance parameters around the knee joint (*Inertia, Damping*, and *Stiffness*). It allows us to define five Markovian operation modes to describe the dynamic interaction process between robot and human knee joint during walking. We present experimental results for a healthy subject wearing a force/impedance controlled knee-exoskeleton. Our Markovian robust approach showed robust stability, high performance, and HRI safety during zero-impedance and robot-assisted walking experiments.

2. SYSTEM DESCRIPTION AND MODELING

In the Laboratory of Robotic Rehabilitation of the University of São Paulo at São Carlos (SP, Brazil), two robotic devices for lower limb rehabilitation were developed: an active knee orthosis (dos Santos et al., 2017), and a modular bilateral lower limb exoskeleton (dos Santos and Siqueira, 2019). The working principle of the orthosis is a rotary SEA consisting of a DC motor (RE 40, graphite brushes, 150 W from Maxon Motor AG, Sachseln, Switzerland) fixed to a worn gear set with 150:1 reduction. When the motor is on, the gear rotates a support piece compressing a customized torsion spring with constant $K_s = 95$ Nm/rad. A magneto-resistant incremental encoder Maxon measures the motor rotation allowing estimation of the worn wheel position. The angular position of the load is measured using an optoelectronic incremental encoder. The output force, given by the spring torque, is measured via Hooke's law from the spring deformation, corresponding to the difference between the angular positions of the worn wheel and the load. On the other hand, the modular exoskeleton consists of lightweight, tubular structures and free joints that allow the movement of the user. The exoskeleton structure allows adjusting the size of the links to align the joints of the human and the exoskeleton. Its modular design enables the use and actuation of one or more joints.

In this study, we used one "leg" of the modular exoskeleton and coupled its knee joint with the rotary actuator of the knee orthosis, as shown in Figure 1. Therefore, the new configuration is composed of three joints: hip, knee, and ankle; with actuation only in the knee joint. Also, two encoders measured the angles of the hip and knee joints. To measure the gait phases during walking, we instrumented the exoskeleton's shoe with three Force Sensitive Resistors (FSRs) placed at heel, toe, and second metatarsus.

2.1 Nominal model of the human-robot dynamics

Consider the human leg interacting with the robotic knee-exoskeleton described in the previous section. Human-robot dynamics in the flexion/extension degree of freedom of the knee is modeled by:

$$J_l\,\ddot{\phi}_k + B_l\,\dot{\phi}_k + G(\phi_k) = \tau_h - \tau_r, \tag{1}$$

where ϕ_k is the sagittal angular position of the knee joint; J_l, B_l, and $G(\phi_k)$ are, respectively, the equivalent inertia, velocity-dependent and gravitational matrices for the human-load system; τ_h and τ_r are torques applied by human and robot, respectively.

The human actuation can be modeled by:

$$\tau_h = K_h(t)(\phi_{eq} - \phi_k) - B_h(t)\dot{\phi}_k, \tag{2}$$

where K_h and B_h are respectively the variable stiffness and damping of the inner motor control.

From (1) and (2),

$$J_l(t)\ddot{\phi}_k + B_H(t)\dot{\phi}_k + K_h(t)\phi_k = -\tau_r - G(\phi_k) + K_h\phi_{eq}, \tag{3}$$

where $B_H(t) = B_l + B_h(t)$. Consider that J_l is a time-varying parameter which value is affected by the contact of the leg with the ground.

The robot torque is given by the Hooke's Law:

$$\tau_r = K_s(\phi_w - \phi_k), \tag{4}$$

where K_s is the elastic constant of the spring and ϕ_w is the position of the worn set. Dynamics of the motor-transmission system is governed by,

$$J_r\,\ddot{\phi}_w + B_r\,\dot{\phi}_w = \tau_{act} + \tau_r, \tag{5}$$

where J_r and B_r are, respectively, the equivalent rotational inertia and damping of the motor-transmission system as defined in dos Santos et al. (2017); and, $\tau_{act} = N_r\tau_m$, is the output torque of the actuator, where N_r is the reduction ratio and τ_m represents the torque generated by the motor.

By using the built-in PI velocity-controller of the motor, we can model its actuation as a pure-velocity source by:

$$\tau_m \approx C_m\omega_m, \tag{6}$$

where C_m is the damping coefficient of the motor and $\omega_m = \frac{d}{dt}\phi_m$ is the motor velocity. Since $\phi_w = N_r^{-1}\phi_m$, the motion of the motor-transmission system is given by:

$$J_r\,\ddot{\phi}_w = B_R\,\omega_m + \tau_r, \tag{7}$$

where $B_R = N_rC_m - N_r^{-1}B_r$.

From (3), (4) and (7), the complete dynamics of the human-robot system is given by (8)-(9). The state vector

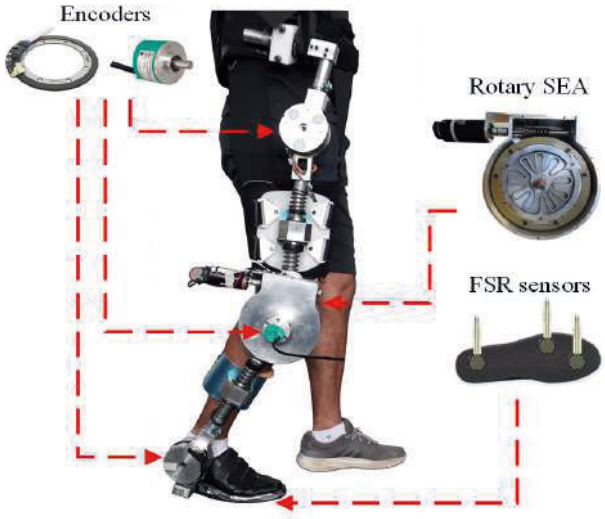

Figure 1. Robotic device configuration. One "leg" of a modular exoskeleton was coupled with a rSEA actuator in order to actuate on the knee joint.

$$\underbrace{\begin{bmatrix}\ddot{\tau}_r\\ \dot{\tau}_r\\ \dot{\phi}_k\end{bmatrix}}_{\dot{\mathcal{X}}_{(t)}} = \underbrace{\begin{bmatrix}-\left(\frac{B_{l(t)}}{J_{l(t)}}\right) & -\left(\frac{K_s(J_l(t)-J_r)+J_rK_l(t)}{J_rJ_l(t)}\right) & 0\\ 1 & 0 & 0\\ -\frac{1}{K_s} & 0 & 0\end{bmatrix}}_{\mathcal{F}_{(t)}}\underbrace{\begin{bmatrix}\dot{\tau}_r\\ \tau_r\\ \phi_k\end{bmatrix}}_{\mathcal{X}_{(t)}} + \underbrace{\begin{bmatrix}K_s\left(\frac{N_rB_RJ_l(t)+J_rB_l(t)}{N_rJ_rJ_l(t)}\right)\\ 0\\ \frac{1}{N_r}\end{bmatrix}}_{\mathcal{B}_{(t)}}\underbrace{\omega_m}_{\mathcal{U}_{(t)}} + \underbrace{\begin{bmatrix}\frac{K_s}{J_{l(t)}} & \frac{K_s}{J_{l(t)}}\\ 0 & 0\\ 0 & 0\end{bmatrix}}_{\mathcal{G}_{(t)}}\underbrace{\begin{bmatrix}G_{(\phi_k)}\\ \tau_{int}\end{bmatrix}}_{\mathcal{V}_{(t)}}, \tag{8}$$

$$\underbrace{\begin{bmatrix}\tau_r\\ \omega_k\\ \phi_k\end{bmatrix}}_{\mathcal{Y}_{(t)}} = \underbrace{\begin{bmatrix}0 & 1 & 0\\ -1/K_s & 0 & 0\\ 0 & 0 & 1\end{bmatrix}}_{\mathcal{C}_2}\underbrace{\begin{bmatrix}\dot{\tau}_r\\ \tau_r\\ \phi_k\end{bmatrix}}_{\mathcal{X}_{(t)}} + \underbrace{\begin{bmatrix}0\\ 1/N_r\\ 0\end{bmatrix}}_{\mathcal{D}_2}\underbrace{\omega_m}_{\mathcal{U}_{(t)}} \tag{9}$$

$\mathcal{X}$ is composed of the robot torque, τ_r, its first derivative, and the knee angle, ϕ_k. The system is controlled through the motor velocity, ω_m. Disturbances are given by the interaction torque, $\tau_{int} = K_h\,(\phi_w - \phi_{eq})$ and gravitational effects, $G_{(\phi_k)}$. Output signals are the robot torque, τ_r, and the knee angular velocity, ω_k, and position, ϕ_k. Note that matrices $\mathcal{F}_{(t)}$, $\mathcal{B}_{(t)}$ and $\mathcal{G}_{(t)}$ are time-varying since they depend on the values of J_l, B_l and K_l, that are not constant during human walking.

The sampling frequency of the system is set to 200 Hz. Therefore, the system in (8) is discretized by,

$$\begin{aligned}\mathcal{X}_{k+1} &= \mathcal{F}_k\,\mathcal{X}_k + \mathcal{B}_k\,\mathcal{U}_k + \mathcal{G}_k\,\mathcal{V}_k,\\ y_k &= \mathcal{C}_2\,\mathcal{X}_k + \mathcal{D}_2\,\mathcal{U}_k,\end{aligned} \tag{10}$$

where $\mathcal{F}_k = I + \eta T_s\mathcal{F}_{(t)}$, $\mathcal{B}_k = \eta T_s\mathcal{B}_{(t)}$, $\mathcal{G}_k = \eta T_s\mathcal{G}_{(t)}$, $\eta = \sum_{k_n=0}^{9}\left[\frac{(T_s\cdot\mathcal{F}_{(t)})^{k_n}}{(k_n+1)!}\right]$, and $T_s = 5$ ms.

2.2 Gait phases and modelling gait as a Markov Chain

Gait is a quasi-cyclic pattern divided into discernible phases. In this study, we divided each foot's strides into the following five: Loading Response (LR), Mid-Stance (MSt), Terminal Stance (TSt), Initial Swing (ISw), and Terminal Swing (TSw). Transitions between phases correspond to the following gait events: Heel Strike (HS), when the first contact between foot and ground occurs; Toe Strike (TS), when there is a complete foot-ground contact; Heel Off (HO) and Toe Off (TO), when the heel and toe lose that contact, respectively; and, Mid Swing (MSw), when the balancing and support legs are adjacent to each other.

We represent the phase sequence by a finite state machine (FSM), where each state corresponds to a given phase. Phase transitions are modeled by a discrete-time Markov chain $\{\theta_k\}_{k=0}^{N-1}$ where $\theta \in \{1,2,3,4,5\}$, being 1: LR, 2: MSt, 3: TSt, 4: ISw, and 5: TSw. The system state (gait phase), θ_k, is estimated based on the values of the FSRs placed on the exoskeleton's shoe and the following rule-based algorithm,

$$\theta_k = \begin{cases} 1 \text{ if } \theta_{k-1} = 5 \text{ and } \mathrm{FSR}_1 \text{ is ON}\\ 2 \text{ if } \theta_{k-1} = 1 \text{ and } \begin{cases}\mathrm{FSR}_1 \text{ is ON}\\ \mathrm{FSR}_{2 \text{ or } 3} \text{ is ON}\end{cases}\\ 3 \text{ if } \theta_{k-1} = 2 \text{ and } \begin{cases}\mathrm{FSR}_1 \text{ is OFF}\\ \mathrm{FSR}_{2 \text{ or } 3} \text{ is ON}\end{cases}\\ 4 \text{ if } \theta_{k-1} = 3 \text{ and all FSR are OFF}\\ 5 \text{ if } \theta_{k-1} = 4 \text{ and } \begin{cases}\text{all FSR are OFF}\\ \phi_h \le 0^o \text{ or } \phi_a \le 0^o\end{cases}\end{cases} \tag{11}$$

where FSR_1, FSR_2, and FSR_3, correspond respectively to the sensors placed at heel, second metatarsus and toe; and, ϕ_h and ϕ_a are respectively the hip and ankle joint angles.

Transitions among phases are determined by the transition matrix $\mathbb{P} \in \mathbb{R}^{5\times5}$ with elements:

$$\mathbb{P}_{ab} = \Pr\left(\theta_{k+1} = b \,|\, \theta_k = a\right), \tag{12}$$

where $\mathbb{P}_{ab}$ is the probability of going from state a to state b satisfying the constraints: $\sum_{b=1}^{5}\mathbb{P}_{ab} = 1$, and $0 \le \mathbb{P}_{ab} \le 1$.

In order to estimate the $\mathbb{P}_{ab}$ values, we asked the subject to walk for five minutes wearing the exoskeleton. Each element $\mathbb{P}_{ab}$ is equal to the ratio between the estimated number of transitions from state a to state b and the estimated number n_a of time samples labeled as state a. Thus, we obtained the following values for $\mathbb{P}_{ab}$,

$$\mathbb{P} = \begin{bmatrix}0.9903 & 0.0097 & 0 & 0 & 0\\ 0 & 0.9947 & 0.0053 & 0 & 0\\ 0 & 0 & 0.9956 & 0.0044 & 0\\ 0 & 0 & 0 & 0.9895 & 0.0105\\ 0.0053 & 0 & 0 & 0 & 0.9947\end{bmatrix}. \tag{13}$$

Markov chains suitably model the stochastic transitions between gait phases. However, they do not take advantage of the regularities in the timing of the gait cycle. In that regard, Ma and Liao (2017) propose the use of a continuous-time semi-Markov process where time intervals for each gait phase have a given probability distribution.

2.3 Modeling the human-exoskeleton system as a DMJLS

Since abrupt changes in knee dynamics occur during gait phase transitions, the system presented in (10) is then expressed as the discrete-time Markovian Jump Linear System given by,

$$\begin{aligned}\mathcal{X}_{k+1} &= \mathcal{F}_{\theta_k,k}\,\mathcal{X}_k + \mathcal{B}_{\theta_k,k}\,\mathcal{U}_k + \mathcal{G}_{\theta_k,k}\,\mathcal{V}_k,\\ \mathcal{Y}_k &= \quad \mathcal{C}_2\,\mathcal{X}_k + \quad \mathcal{D}_2\,\mathcal{U}_k,\end{aligned} \tag{14}$$

where the notation $\mathcal{F}_{\theta_k,k}$ indicates that the matrix $\mathcal{F}_k$ is governed by the Markov chain θ_k, whose transitions are defined by (11) and the probability of transitions among phases are determined by (13).

3. ESTIMATION OF THE TIME-VARYING DYNAMICS OF THE KNEE DURING WALKING

Based on the approach used in Lee and Hogan (2015), this section explains the ensemble-based method employed to estimate the time-varying knee-exoskeleton dynamics during walking. Assuming that every gait cycle has the same

time-varying dynamics, this method uses an ensemble set composed by the gait signals segmented in strides based on the HS events, normalizing the length of all strides to the mean stride duration.

3.1 IRF of the human-exoskeleton system during walking

From (14), the time-varying dynamics of the knee-exoskeleton system during walking can be rewritten in the following vector auto-regressive form,

$$\mathcal{Y}_i = T_s \sum_{j=1}^{L} h_{i,j}\, \mathcal{U}_{i-j}, \tag{15}$$

for all $i = 1, ..., N_s$, where N_s is the mean stride duration; $h_{i,j} = -\mathcal{D}_2 + \left[\mathcal{C}_2 \left(\mathcal{F}_{\theta_i,i-j}\right)^{j-1} \left(\mathcal{B}_{\theta_i,i-j} + \mathcal{G}_{\theta_i,i-j}\right)\right]$ is the time-varying Impulse Response Function (IRF) of the system within a finite lag length L, and $\theta_i \in \{1, 2, 3, 4, 5\}$. Since the system has several inputs and disturbances, $\mathcal{Y}_i$ is composed by the effects of both inputs,

$$\mathcal{Y}_i = \underbrace{T_s \sum_{j=1}^{L} h^{\eta}_{i,j}\, \mathcal{U}_{i-j}}_{y^{\eta}_i} + \underbrace{T_s \sum_{j=1}^{L} h^{0}_{i,j}\, \mathcal{V}_{i-j}}_{y^{0}_i} \tag{16}$$

where $\mathcal{Y}^0_i$ is the nominal trajectory due to inputs G and τ_{int}; and, $\mathcal{Y}^{\eta}_i$ is the effect of the robot perturbations.

3.2 Ensemble-based IRF estimation

Given a set of R realizations of the gait cycle and assuming that are subject to the same time-varying dynamics, the nominal component $\mathcal{Y}^0_i$ corresponds to the average value of the observations across the R realizations. The estimated output $\hat{\mathcal{Y}}^{\eta}_i$, resultant of the robot perturbations, can be obtained by,

$$\hat{\mathcal{Y}}^{\eta}_i = \mathcal{Y}_i - \mathcal{Y}^0_i = T_s \sum_{j=1}^{L} h^{\eta}_{i,j}\, \mathcal{U}_{i-j}. \tag{17}$$

Estimates of the IRF $\hat{h}^{\eta}_i$ can be computed by:

$$\hat{h}^{\eta}_i = \frac{1}{T_s} \left[\mathbf{\Phi_{uu}}(i)\right]^{-1} \mathbf{\Phi_{yu}}(i), \tag{18}$$

where $\mathbf{\Phi_{yu}}(i) \in \mathbb{R}^{L\times 1}$ represents the input-output cross-correlation estimate with elements,

$$\hat{\phi}_{yu}(i, -j) = \frac{1}{R} \sum_{r=1}^{R} \mathcal{Y}^{\eta}_i\, \mathcal{U}_{i-j}, \qquad \text{for } 1 \le j \le L, \tag{19}$$

$\mathbf{\Phi_{uu}}(i) \in \mathbb{R}^{L\times L}$ represents the input auto-correlation function estimate with elements,

$$\hat{\phi}_{uu}(i-j, j-m) = \frac{1}{R} \sum_{r=1}^{R} \mathcal{U}_{i-m}\, \mathcal{U}_{i-j}\,. \tag{20}$$

3.3 Experimental Characterization

We instructed a healthy subject (male, 28 years old, 177 cm, 82 kg) to wear the robotic device and to walk on a treadmill on his self-selected walking speed. After one minute of walking under zero-impedance actuation, the robot applied a mechanical perturbation to the knee joint for the next eight minutes. This perturbation comprises a low-pass filtered Gaussian white noise added in the motor velocity signal. Peak-to-peak values of the torque perturbations were ±250 rad/s.

For each output signal in $\mathcal{Y}$ (τ_r, ω_k, and ϕ_k), we estimated its corresponding IRF ($\hat{h}^{\tau_r}$, $\hat{h}^{\omega_l}$, and $\hat{h}^{\phi_l}$) at every 5 ms and then smoothed the estimates using a moving average with a window of 0.1 sec ($N_w = 40$), by

$$\bar{\hat{h}}_i = \frac{1}{N_w} \sum_{j=i-N_w/2}^{i+N_w/2} \hat{h}_j. \tag{21}$$

Representative IRF estimates for each phase were computed by averaging the IRFs obtained during that phase,

$$\hat{h}^{\theta}_i = \frac{1}{n_\theta} \sum_{\theta_i=\theta} \bar{\hat{h}}_i. \tag{22}$$

Figure 2 presents graphical results of the IRF estimation for the outputs ϕ_k and τ_r.

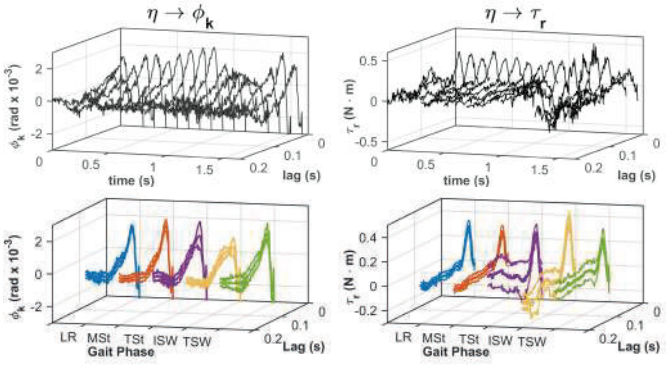

Figure 2. Representative IRF estimates along normalized gait for ϕ_k (left) and τ_r (right). (top) Smoothed IRF estimates for a time step of 80 ms. (bottom) Representative IRF for each gait phase. Each phase is represented by different colored lines (LR: blue, MSt: red, TSt: magenta, ISW: yellow, and TSW: green).

From (8), we can determine the transfer function between signals ϕ_k and τ_r as the 2nd-order system,

$$\mathcal{Z}(s) = \frac{\phi_k(s)}{\tau_r(s)} = \frac{K_s \left(B_R \frac{J_l}{J_r} + \frac{B_l}{N_r}\right)}{J_l\, s^2 + B_l\, s + K_l + K_s \left(1 + \frac{J_l}{J_r}\right)} \tag{23}$$

with time-varying parameters $J_{l(i)}$, $B_{l(i)}$, and $K_{l(i)}$.

Note that the signal $\hat{h}^{\phi_l}(i)$ is the output of the system $\mathcal{Z}(s)$ when the signal $\hat{h}^{\tau_r}(i)$ is the input of the system. We estimate the values for J_l, B_l, and K_l that better approximates $\mathcal{Z}(s)$ for each input-output pair $\left(\hat{h}^{\tau_r}(i), \hat{h}^{\phi_k}(i)\right)$.

Figure 3 presents results for the estimation of the knee stiffness. Table 1 presents the values obtained for the three parameters (J_l, B_l and K_h) for each phase.

These values should be considered as nominal values subject to uncertainties within each phase, expressed by,

$$\begin{aligned} J^{\delta}_{l,\theta_k,k} &= J_r + J^{\delta}_{h,\theta_k,k}, \\ B^{\delta}_{l,\theta_k,k} &= B_r + B^{\delta}_{h,\theta_k,k}, \\ K^{\delta}_{l,\theta_k,k} &= K^{\delta}_{h,\theta_k,k} \end{aligned} \tag{24}$$

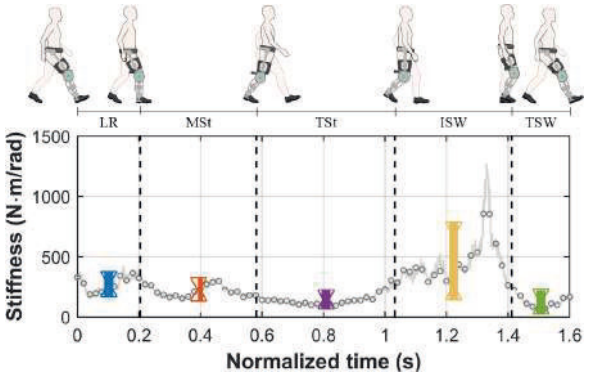

Figure 3. Estimated knee stiffness during gait cycle. Representative values for each phase are shown using the same color code as in the previous figure.

Table 1. Estimated human parameters

Phase	Markov mode	J_l	B_l	K_h
LR	$\theta_k = 1$	0.001	1.5	275
MSt	$\theta_k = 2$	0.001	0.8	229
TSt	$\theta_k = 3$	0.005	1.0	145
ISW	$\theta_k = 4$	>0.10	>3.0	465
TSW	$\theta_k = 5$	0.001	2.0	129

where $J^{\delta}_{h,\theta_k,k}$, $B^{\delta}_{h,\theta_k,k}$, and $K^{\delta}_{h,\theta_k,k}$ are uncertain human impedance parameters subjects to Markovian jumps according to Table 1. Hence, the DJMLS in (14) is subject to the following uncertain state matrices,

$$\begin{aligned}\bar{\mathcal{F}}^{\delta}_{\theta_k,k} &= \mathcal{F}_{\theta_k,k} + \delta\mathcal{F}_{\theta_k,k},\\ \bar{\mathcal{B}}^{\delta}_{\theta_k,k} &= \mathcal{B}_{\theta_k,k} + \delta\mathcal{B}_{\theta_k,k}\end{aligned} \tag{25}$$

4. CONTROL DESIGN

In this section, we present the Robust Regulator Discrete-time Markovian Jump Linear System (RR-DMJLS). To eliminate the steady-state torque error during tracking a reference torque τ^d_k, we augmented the model in (14) by including an integral action x^i_k,

$$\begin{aligned}\underbrace{\begin{bmatrix}\bar{x}_{k+1}\\ x^i_{k+1}\end{bmatrix}}_{x_{k+1}} &= \underbrace{\begin{bmatrix}\bar{\mathcal{F}}^{\delta}_{\theta_k,k} & 0\\ C_a T_s & 1\end{bmatrix}}_{F^{\delta}_{\theta_k,k}}\underbrace{\begin{bmatrix}\bar{x}_k\\ x^i_k\end{bmatrix}}_{x_k} + \underbrace{\begin{bmatrix}\bar{\mathcal{B}}^{\delta}_{\theta_k,k}\\ 0\end{bmatrix}}_{B^{\delta}_{\theta_k,k}} u_k\\ &+ \underbrace{\begin{bmatrix}\bar{\mathcal{G}}_{\theta_k,k}\\ 0\end{bmatrix}}_{G_{\theta_k,k}} v_k + \underbrace{\begin{bmatrix}0\\ T_s\end{bmatrix}}_{B^d_{\theta_k,k}}\tau^d_k,\end{aligned} \tag{26}$$

where $C_a = [0\ -1\ 0]$. Therefore, the discrete-time system in (26) can be rewritten as:

$$\begin{aligned}x_{k+1} &= (F_{\theta_k,k} + \delta F_{\theta_k,k})x_k + (B_{\theta_k,k} + \delta B_{\theta_k,k})u_k\\ &\quad + G_{\theta_k,k}w_k + B^d_{\theta_k,k}\tau^d_k,\\ y_k &= C_2 x_k + D_2 u_k,\end{aligned} \tag{27}$$

for all $k = 0, ..., N-1$, where $C_2 = [\mathcal{C}_2\ 0]$.

Uncertain matrices $\delta F_{\theta_k,k}$ and $\delta B_{\theta_k,k}$ are defined as,

$$[\delta F_{\theta_k,k}\ \delta B_{\theta_k,k}] = H_{\theta_k,k}\Delta_{\theta_k,k}\begin{bmatrix}E_{F_{\theta_k,k}} & E_{B_{\theta_k,k}}\end{bmatrix} \tag{28}$$

where $H_{\theta_k,k} \in \mathbb{R}^{4\times 1}$, $E_{F_{\theta_k,k}} \in \mathbb{R}^{1\times 4}$, $E_{B_{\theta_k,k}} \in \mathbb{R}^{1\times 1}$, are known matrices, and $\Delta_{\theta_k,k} \in \mathbb{R}^{1\times 1}$ which is a contraction such that $\| \Delta_{\theta_k,k} \| \leq 1$.

4.1 RR-DMJLS for Knee-exoskeleton

Consider the robust control problem of regulating the DJMLS in (26) subject to the parametric uncertainties in (28). To achieve the solution to this problem is used the min-max optimization problem:

$$\min_{x_{k+1},u_k}\ \max_{\delta F_{\theta_k,k},\delta B_{\theta_k,k}} \{\mathcal{J}^{\mu}_k\}, \tag{29}$$

where $\mathcal{J}^{\mu}_k$ is a quadratic functional given by,

$$\begin{aligned}\mathcal{J}^{\mu}_k &= \begin{bmatrix}x_{k+1}\\ u_k\end{bmatrix}^T\begin{bmatrix}\Psi_{\theta_k,k+1} & 0\\ 0 & R_{\theta_k,k}\end{bmatrix}\begin{bmatrix}x_{k+1}\\ u_k\end{bmatrix} +\\ &\left\{\begin{bmatrix}0 & 0\\ I & -B^{\delta}_{\theta_k,k}\end{bmatrix}\begin{bmatrix}x_{k+1}\\ u_k\end{bmatrix} - \begin{bmatrix}-I\\ F^{\delta}_{\theta_k,k}\end{bmatrix}x_k\right\}^T\begin{bmatrix}Q_{\theta_k,k} & 0\\ 0 & \mu I\end{bmatrix}\{\bullet\}\end{aligned} \tag{30}$$

where $\Psi_{\theta_k}(k+1) = \sum_{\theta_k=1}^{5} P_{\theta_k,k+1}\cdot p_{\theta_k,k+1}$; $P_{\theta_k,k} \succ 0$ is a positive definite matrix; $Q_{\theta_k,k} \succ 0$, and $R_{\theta(k),k} \succ 0$ are semi-definite weighting matrices. Table 2 shows the algorithm that guarantees the optimal state-control sequence $\{x^*_{\mu,k+1}, u^*_{\mu,k}\}^{N-1}_{k=0}$ for an instant k and state θ.

Table 2. Robust Regulator for DMJLS

Initial Conditions:
Set $x_0, \theta_0, \mathbb{P}, P_{\theta_k}(N) \succ 0, \forall\theta_k \in \{1, ..., s\}$.
Step 1: (*Backward*). Calculate, for all $k = N-1, \ldots, 0$,

$$\begin{bmatrix}L_{\theta_k,k} & K_{\theta_k,k} & P_{\theta_k,k}\end{bmatrix}^T = \begin{bmatrix}0&0&0&0&I&0\\ 0&0&0&0&0&I\\ 0&0&-I&\hat{F}_{\theta_k,k}&0&0\end{bmatrix}$$
$$\cdot\begin{bmatrix}\Psi^{-1}_{\theta_k,k+1}&0&0&0&I&0\\ 0&R^{-1}_{\theta_k,k}&0&0&0&I\\ 0&0&Q^{-1}_{\theta_k,k}&0&0&0\\ 0&0&0&\mathcal{W}_{\theta_k,k}&\hat{I}&-\hat{B}_{\theta_k,k}\\ I&0&0&\hat{I}^T&0&0\\ 0&I&0&-\hat{B}^T_{\theta_k,k}&0&0\end{bmatrix}^{-1}\begin{bmatrix}0\\0\\-I\\ \hat{F}_{\theta_k,k}\\0\\0\end{bmatrix}$$

with the following auxiliary matrices:

$$\Psi_{\theta_k,k+1} = \sum_{j=1}^{s} P_{j,k+1}p_{ij},\quad \hat{\lambda}_{\theta_k,k} > \left\|\mu H^T_{\theta_k,k}H_{\theta_k,k}\right\|,$$
$$\hat{F}_{\theta_k,k} = \begin{bmatrix}F_{\theta_k,k}\\ E_{F_{\theta_k,k}}\end{bmatrix},\quad \hat{B}_{\theta_k,k} = \begin{bmatrix}B_{\theta_k,k}\\ E_{B_{\theta_k,k}}\end{bmatrix},\quad \hat{I} = \begin{bmatrix}I\\0\end{bmatrix},$$
$$\mathcal{W}_{\theta_k,k} = \begin{bmatrix}\mu^{-1}I - \hat{\lambda}^{-1}_{\theta_k,k}H_{\theta_k,k}H^T_{\theta_k,k} & 0\\ 0 & \hat{\lambda}^{-1}_{\theta_k,k}I\end{bmatrix},$$

Step 2: (*Forward*). Obtain, for each $k = 0, \ldots N-1$,
$\begin{bmatrix}x^*_{k+1}\\ u^*_k\end{bmatrix} = \begin{bmatrix}L_{\theta_k,k}\\ K_{\theta_k,k}\end{bmatrix}x^*_k$.

In this formulation, μ is a penalty parameter responsible for guaranteeing the robustness of RR-DMJLS. Therefore, if all states of the system are available and $\mu \to +\infty$, $\mathcal{W}_{i,k} \to 0$. The DMJLS closed-loop response is given by:

$$\begin{cases}L_{\theta_k,k} = F_{\theta_k,k} + B_{\theta_k,k}K_{\theta_k,k}\\ E_{F_{\theta_k,k}} + E_{B_{\theta_k,k}}K_{\theta_k,k} = 0.\end{cases} \tag{31}$$

Let $\mu = 1\cdot 10^{12}$ and $\lambda_{\theta_k,k} = 1\cdot 10^{12}$ in order to satisfy (31). In addition, we set $P_{\theta_k,k}(N) = I_{4\times 4}$, $R_{\theta_k,k} = 1$ and $Q_{\theta_k,k} = I_{4\times 4}$ for $\theta_k \in \{1,2,3,4,5\}$; $\mathbb{P}$ as defined in (13), and the following uncertainty parameter matrices:

$$\left.\begin{aligned}H_{\theta_k,k} &= [10\ 10\ 10\ 10]^T\\ E_{B_{\theta_k,k}} &= -5\end{aligned}\right\}\ \text{for } \theta_k \in \{1,2,3,4,5\}.$$

$$
\begin{aligned}
E_{F_{1,k}} &= [-120\ -2100\ 425\ 13950]\,,\\
E_{F_{2,k}} &= [-60\ -1725\ 445\ 24960]\,,\\
E_{F_{3,k}} &= [-40\ -1500\ 380\ 26138]\,,\\
E_{F_{4,k}} &= [-30\ -1100\ 360\ 15000]\,,\\
E_{F_{5,k}} &= [-40\ -2600\ 470\ 25000]\,. \qquad (32)
\end{aligned}
$$

Consequently, by using the RR-DMJLS presented in Table 2, we obtain the following control law:

$$u_k = K_{\theta_k,k} x_k, \qquad (33)$$

where $K_{\theta_k,k}$ are control gain obtained for each Markovian state θ_k, as presented in Table 3.

Table 3. Control Gains

Markov modes	$K_{\theta_k,1}$	$K_{\theta_k,2}$	$K_{\theta_k,3}$	$K_{\theta_k,4}$	Gains
$\theta_k = 1$	-24	-420	85	2790	$K_{1,k}$
$\theta_k = 2$	-12	-345	90	4992	$K_{2,k}$
$\theta_k = 3$	-8	-300	75	5200	$K_{3,k}$
$\theta_k = 4$	-6	-220	72	3000	$K_{4,k}$
$\theta_k = 5$	-8	-520	95	5000	$K_{5,k}$

5. EXPERIMENTAL RESULTS

In this section, we present results for two applications of the proposed approach in the control of the exoskeleton: use of the RR-DMJLS for torque control; and, impedance control using the torque control as an internal loop.

5.1 Torque Control

We performed two experiments to evaluate the response of the torque controller in two extreme operation modes: high human impedance (as in *Initial-Swing* (ISw) when $\theta_k = 4$), and low human impedance (as in *Terminal-Swing* (TSw) when $\theta_k = 5$). We present results for two different torque references, a sine wave, and a square wave. With respective periods of 3 s and 4 s, both reference signals have 2.5 N·m of amplitude. In both experiments, the subject wore the exoskeleton on his right side and stood on the left foot on a block providing clearance between the right foot and the ground. For the low impedance case, we asked the user to relax the leg and allow the robot to lead the movement. For the high impedance case, we asked the user to oppose the movement intending to maintain the knee joint in a neutral position. For both impedance configuration, we evaluated two sets of control gains: $K_{4,k}$ and $K_{5,k}$.

Figure 4 shows the torque control response for the two Markovian operation modes when tracking sinusoidal and square references. Despite the performance for torque tracking is similar in both modes, the control strategy obtained better performance when the selected gain matches its operation mode.

Quantitative evaluation of the controller performance is computed by using the root mean square (RMS) error between desired and measured torque, defined as:

$$RMS\{e_\tau\} = \frac{1}{c}\sum_{k=1}^{c} \left|\frac{\tau_k^d - \tau_r}{\max \tau_k^d}\right| \cdot 100\%, \qquad (34)$$

where c is the number of samples in each test. Thus, the RMS error obtained for high and low human impedance is presented in Table 4.

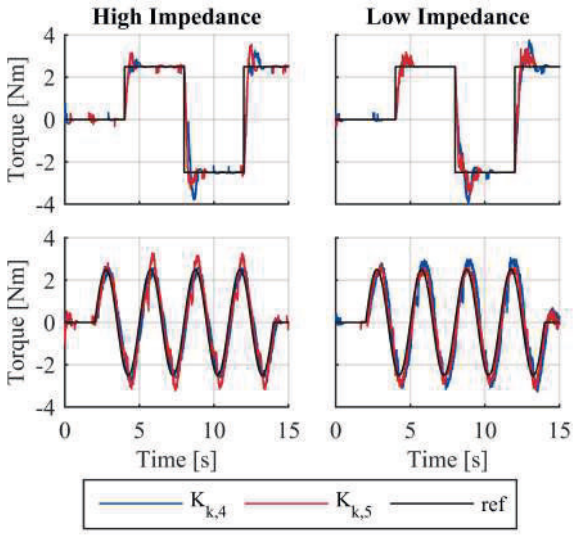

Figure 4. Force control response for high (left) and low (right) impedance. Mode 4 in blue, Mode 5 in red, reference signal in black.

Table 4. RMS Force Error

Reference	Step		Sine	
Markov modes	$K_{4,k}$	$K_{5,k}$	$K_{4,k}$	$K_{5,k}$
High human-impedance	12.1%	14.1%	14.1%	15%
Low human-impedance	15.2%	10.1%	12.6%	9.1%

5.2 Impedance Control

For an adequate human-robot interaction, we defined the robot torque by the following impedance control law:

$$\tau_r^d = K_v\,(\phi_k^d - \phi_k) - B_v\,\omega_k, \qquad (35)$$

where τ_r^d is the desired torque, ϕ_k^d is the desired trajectory for the knee angular position. K_v and B_v are the virtual stiffness and damping, respectively.

We performed an experiment using the RR-DMJLS as inner-loop torque control during impedance controlled movements. To generate the desired trajectory ϕ_k^d of the impedance control, the subject walked on the treadmill for 1 minute at a comfortable speed of 2 m/s with zero-impedance configuration ($K_v = 0$ Nm/rad and $B_v = 0$ Nms/rad). ϕ_k^d corresponds to the average of the stride-segmented, time-normalized angular position of the knee (similar to $\mathcal{Y}_i^0$ is Section 3.2). Once ϕ_k^d was defined, we asked the subject to walk on the treadmill for 60 s at 2 m/s, with $K_v = 30$ Nm/rad and $B_v = 0.5$ Nms/rad.

Figure 5 shows representative temporal responses for the force and impedance control during a walking experiment. Notice that the torque tracking performance is similar for all Markov modes despite the abrupt transitions between them. Also, notice how the variations in the control signal due to the phase transitions do not compromise the robust stability and performance of the control system.

Finally, in order to quantify the performance of the proposed controller, we compute the real stiffness, K_{vr}, and damping, B_{vr}, generated by the controller, as given by:

$$K_{vr} = \frac{RMS\{\tau_{K_v}\}}{RMS\{e_\phi\}} \quad \text{and} \quad B_{vr} = \frac{RMS\{\tau_{B_v}\}}{RMS\{e_\omega\}} \qquad (36)$$

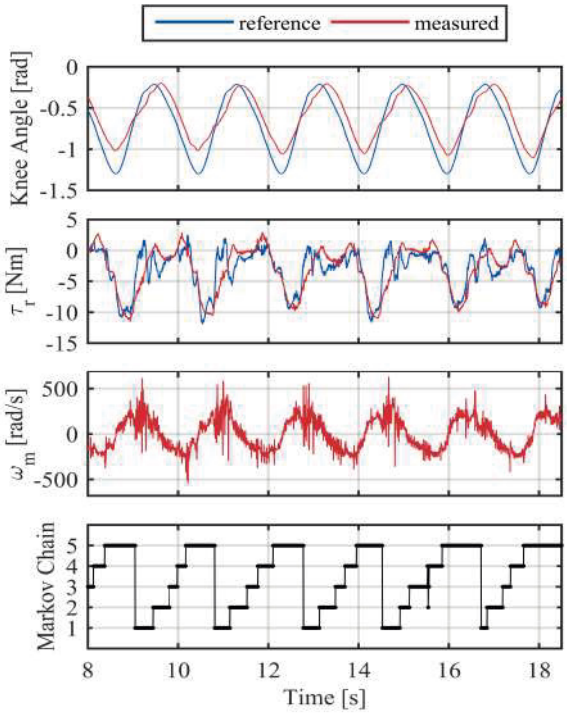

Figure 5. Impedance control response. Graphs show (top) desired, ϕ_k^d, and measured, ϕ_k, knee angular position; (top-middle) desired, τ_r^d, and measured, τ_r, robot torque; (bottom-middle) control signal ω_m; and, (bottom) Markov chain, θ_k, of the modeled process.

where $\tau_{K_v} = \tau_r - B_w e_\omega$, is the torque generated by the virtual stiffness K_v, with $e_\omega = -\omega_k$; and, $\tau_{B_v} = \tau_r - K_v e_\phi$ is the torque generated by the virtual damping B_v, with $e_\phi = \phi_k^d - \phi_k$. The error between virtual and real impedance parameters is calculated by $e_{K_v} = |(K_v - K_{vr})(K_v)| \cdot 100\%$, and $e_{B_v} = |(B_v - B_{vr})/(B_v)| \cdot 100\%$.

Impedance control using RR-DMJLS presents high stiffness and damping accuracy by considering the variability of the human impedance parameters during walking, with $e_{K_v} = 2.82\%$, and $e_{B_v} = 0.73\%$.

6. CONCLUSION

In this paper, we presented the design and implementation of an impedance control based on a robust Markovian torque controller. We modeled human-robot interaction dynamics during walking using a discrete-time Markov jump linear system (DMJLS) and designed a robust regulator for DMJLS to control the robot torque. We assumed parametric uncertainties introduced by the change of behavior human dynamic during walking. Experimental results on a knee-exoskeleton are also presented and showed that our proposal guarantees robust stability and performance in the human-robot interaction control.

REFERENCES

K. Anam and A. Al-Jumaily. Active exoskeleton control systems: State of the art. *Procedia Engineering*, 41:988–994, 2012.

A. Calanca and P. Fiorini. Impedance control of series elastic actuators based on well-defined force dynamics. *Robotics and Autonomous Systems*, 96:81–92, 2017.

A. Calanca, R. Muradore, and P. Fiorini. A review of algorithms for compliant control of stiff and fixed-compliance robots. *IEEE/ASME Transactions on Mechatronics*, 21(2):613–624, 2016.

J. Cerri and M. Terra. Recursive robust regulator for discrete-time Markovian jump linear systems. *IEEE Trans. on Automatic Control*, 62(11):6004–6011, 2017.

W. M. dos Santos and A. A. G. Siqueira. Design and control of a transparent lower limb exoskeleton. In *Wearable Robotics: Challenges and Trends*, pages 175–179. Springer, 2019.

W. M. dos Santos, G. A. Caurin, and A. A. G. Siqueira. Design and control of an active knee orthosis driven by a rotary series elastic actuator. *Control Engineering Practice*, 58:307–318, 2017.

N. Hogan. Impedance control: An approach to manipulation: Parts I-III. *Journal of Dynamic Systems, Measurement, and Control*, 107(1):17–24, March 1985.

A. L. Jutinico, J. C. Jaimes, F. M. Escalante, J. C. Perez-Ibarra, M. H. Terra, and A. A. G. Siqueira. Impedance control for robotic rehabilitation: A robust Markovian approach. *Frontiers in Neurorobotics*, 11:43, 2017.

K. Kong, J. Bae, and M. Tomizuka. Control of rotary series elastic actuator for ideal force-mode actuation in human–robot interaction applications. *IEEE/ASME transactions on mechatronics*, 14(1):105–118, 2009.

P. A. Lasota, T. Fong, J. A. Shah, et al. A survey of methods for safe human-robot interaction. *Foundations and Trends in Robotics*, 5(4):261–349, 2017.

H. Lee and N. Hogan. Time-varying ankle mechanical impedance during human locomotion. *IEEE Transactions on Neural Systems and Rehabilitation Engineering*, 23(5):755–764, 2015.

X. Li, Y. Pan, G. Chen, and H. Yu. Adaptive human–robot interaction control for robots driven by series elastic actuators. *IEEE Transactions on Robotics*, 33(1):169–182, February 2017.

H. Ma and W. Liao. Human gait modeling and analysis using a semi-Markov process with ground reaction forces. *IEEE Transactions on Neural Systems and Rehabilitation Engineering*, 25(6):597–607, 2017.

J. Mehling, J. Holley, and M. O'Malley. Leveraging disturbance observer based torque control for improved impedance rendering with series elastic actuators. In *2015 IEEE/RSJ International Conference on Intelligent Robots and Systems*, pages 1646–1651. IEEE, 2015.

S. Oh and K. Kong. High-precision robust force control of a series elastic actuator. *IEEE/ASME Transactions on Mechatronics*, 22(1):71–80, 2016.

N. Paine, J. Mehling, J. Holley, N. Radford, G. Johnson, C. Fok, and L. Sentis. Actuator control for the nasa-jsc valkyrie humanoid robot: A decoupled dynamics approach for torque control of series elastic robots. *Journal of Field Robotics*, 32(3):378–396, 2015.

J. Pérez-Ibarra, A. Alarcón, J. C. Jaimes, F. Ortega, M. H. Terra, and A. Siqueira. Design and analysis of H_∞ force control of a series elastic actuator for impedance control of an ankle rehabilitation robotic platform. In *2017 American Control Conference*, pages 2423–2428, 2017.

H. Yu, S. Huang, G. Chen, Y. Pan, and Z. Guo. Human–robot interaction control of rehabilitation robots with series elastic actuators. *IEEE Transactions on Robotics*, 31(5):1089–1100, October 2015.